https://doi.org/10.5194/essd-2026-398
Preprint. Discussion started: 11 June 2026

Open Access Earth System Science Data Discussions

Regional high-resolution eddy model and data fusion dataset EFGO

Chunling Zhang[1], Aoran Sun[1], Kefeng Mao[2], Zenghong Liu[3], Penghao Wang[4], Lifu Fu[1], Yuhang Zhu[1], Jiahui Fan[1]

[1]College of Marine Science, Shanghai Ocean University, Shanghai 201306, China
[2]College of Advanced Interdisciplinary Studies, National University of Defense Technology, Nanjing 210014, China
[3]State Key Laboratory of Satellite Ocean Environment Dynamics, Second Institute of Oceanography, Ministry of Natural Resources, Hangzhou 310012, China
[4]Marine Science and Technology College, Zhejiang Ocean University, Zhoushan 316022, China

Correspondence to: Kefeng Mao (maokefeng@nudt.edu.cn), Zenghong Liu (zliu@sio.org.cn), Chunling Zhang (clzhang@shou.edu.cn)

Abstract. By integrating a machine learning model for eddy reconstruction with an optimized objective analysis method, this study developed a daily dataset (Eddy Model Fusion Gradient Optimal Interpolation Data, EFGO) target for mesoscale eddy dynamics with a spatial resolution of 1/16 ° in the Pacific western boundary current region (114 °E -135 °E, 15 °N -35 °N). The iterative correction of background, quality control of multi-source data, gradient constraints on background error in the fusion method, and repeated validation of adjustable parameters collectively ensure the reliability of the dataset. More than 70% of the theoretical analysis errors are less than 0.1, with a maximum not exceeding 0.5. Through cross-validation with other datasets, EFGO demonstrates finer feature extraction for mesoscale processes. Compared with in-situ Argo profiles, the maximum temperature and salinity biases of EFGO do not exceed 0.5 ℃ and 0.05, respectively, which are smaller than those of other eddy-resolving datasets such as GLORYS12 and HYCOM. EFGO aligns more closely with the observations than GLORYS12 and HYCOM along both Argo and WOD observation sections. Characterized primarily by enhanced eddy representation, this dataset includes multiple variables such as temperature, salinity, thermocline, sound channel depth, and eddy parameters. It provides crucial data support for the comprehensive and detailed description of refined marine environmental features. Furthermore, it is applicable in various fields including ecological dynamics and military oceanography.

1. Introduction

Mesoscale eddies, characterized by intense geostrophic strain rates, play important roles in ecological and biogeochemical processes through their contributions to vertical nutrient transport and alteration of the underwater light field (Falkowski et al., 1991; Klein and Lapeyre, 2009; Dong et al., 2017). Mesoscale eddies obtain kinetic energy from large - scale currents and subsequently dissipate to submesoscale or finer - scale processes in the slope regions via combined shear and baroclinic instability (Okkonen et al., 2003). The real - time evolution of eddies will lead to the generation of submesoscale processes with kilometer - scale spatial resolutions (McWilliams, 2016). This dynamic interaction and fine eddy structure display require observational systems with high spatio - temporal synchronization and enhanced resolution capabilities.

With the continuous development of advanced technologies such as satellite remote sensing, profiling floats, and underwater gliders, the integration of surface and subsurface observations enables the acquisition of in-situ profiles within certain mesoscale eddies, thereby allowing for the real-time visualization of their three-dimensional structures.

https://doi.org/10.5194/essd-2026-398
Preprint. Discussion started: 11 June 2026

Open Access Earth System Science Data Discussions

For instance, combined observations with mooring arrays have mapped the full-depth 3D structure of anticyclonic and cyclonic eddy pairs in the South China Sea, revealing significantly tilted geometric features of the eddy central axis (Zhang et al., 2016). Using research vessels equipped with profiling instruments, the complete 3D structure of an eddy can be reconstructed from consecutive observations over several days (Sandalyuk et al., 2020; Scott, 2019). However, observations of internal eddy obtained via combined observation methods are usually fragmented and low spatiotemporal resolution. Consequently, they are insufficient to depict the complete three-dimensional thermohaline structure and are subject to evident temporal and spatial mixing effects. Therefore, many scholars currently utilize multi-year observational data to reconstruct the mean feature of eddies in a specific region through composite analysis (Chaigneau et al., 2011; Zhang et al., 2013). This method has been applied to various areas, such as the Northwest Subtropical Pacific (Yang et al., 2013), the Kuroshio Extension (Dong et al., 2017), and the South China Sea (Qingyou et al., 2018). Although composite analysis can reveal the average-state features of eddies with varying polarities across different regions, it fails to capture the detailed characteristics of individual eddies.

In recent years, the rapid development of machine learning models has provided technical support for the reconstruction of eddy internal structures. Leveraging the powerful nonlinear fitting capabilities of deep learning, it is now possible to reconstruct 3D structures with high spatiotemporal resolution in eddy regions (Zhu et al., 2025; Ma et al., 2023; Zhang et al., 2025; Ma et al., 2024). Incorporating physical laws, such as thermodynamic equations and geostrophic relations, as constraints into the model training process can enhance the model's reliability and physical consistency (Zhang et al., 2025; Asdar et al., 2024; Ma et al., 2023). Due to technical limitations, single-source data has its own constraints and applicable scope. Individual data can only reflect certain ocean environmental features at its specific temporal and spatial scales. Even eddy-enhanced observations and reconstructions face limitations in spatiotemporal mismatches with the oceanic background environment. To construct the high-resolution marine environmental datasets through multi-source fusion techniques, a more comprehensive and precise description of the ocean state can be provided. The comprehensive dataset, China Global Ocean Fusion Dataset (CGOF1.0), integrates over 40 publicly shared global ocean data. By leveraging AI technologies, combined with physical models, it addresses the challenge of reconstructing sparse observational data, achieving a spatial resolution of 10km (https://www.cmoc-china.cn/pages/CGOF.html). Concurrently, datasets with high precision tailored to specific oceanic dynamical phenomena are continually being published (Xing et al., 2023; Ma et al., 2024). Yet, the eddy-enhanced datasets with high-resolution are still scarce.

Developed as a data assimilation method, the gradient-dependent optimal interpolation can automatically adjust the correlation scales of background error covariance matrix, thereby more fully extracting observational information from various data sources. According to horizontal gradient variations in mesoscale systems， this study improves the anisotropic correlation scale model in the gradient-dependent optimal interpolation. Employing this optimized data fusion method, multi-source data including reconstructed profiles, satellite observations, Argo profiles, and historical shipboard measurements are integrated to generate a high-resolution and eddy-enhanced dataset EFGO (Eddy Model Fusion Gradient Optimal Interpolation Data). In this dataset, the eddy internal profiles reconstructed by a machine learning model combining physical constraints with data-driven approaches serve as one of the important data sources. It makes the dataset refined in eddy regions, holding significant value for oceanographic research and environmental monitoring.

2. Materials and method

2.1 Observations

Seven categories of data are collected in this study, including in-situ profiles from historical datasets and sea surface

https://doi.org/10.5194/essd-2026-398
Preprint. Discussion started: 11 June 2026

observations by satellite (Table 1, Fig. 1). Argo temperature and salinity profiles are categorized into three types: profiles within the mesoscale eddies are used to reconstruct eddy structure by machine learning; a section profiles are selected to compare the fusion results; the others are composited in data fusion. GTSPP (Global Temperature and Salinity Profile Programme) profiles are used in data fusion by removing duplicate Argo observations. CTD (Conductivity-Temperature-Depth), XBT (Expendable Bathythermograph), XCTD (Expendable Conductivity-Temperature-Depth), moored buoy (MRB), and drifting buoy observation data from WOD (World Ocean Database) are chosen to be used in data fusion and comparison. Satellite Sea surface temperature (SST) and sea surface salinity (SSS) products are employed to compensate for the lack of sea surface data. The satellite altimeter data, sea level anomaly (SLA) and surface velocity are respectively used for eddy structure reconstruction and eddy detection.

Table 1. Observations used in this study.

Dataset	Variables	Time	Area	Purpose
Argo	temperature, salinity	1997.01.01-2024.12.31, 2024.01.01-2025.06.30, 2025.01.19-2025.03.03	15 °N- 35 °N , 114 °E-135 °E	eddy reconstruction, data fusion, and results verification
GTSPP	temperature, salinity	2024.01.01-2025.06.30		data fusion
WOD	temperature, salinity	2024.01.01-2025.06.30, 2024.09.07-2024.09.25		data fusion, results verification
SST	temperature	1981.01.01-2024.12.31, 2024.01.01-2025.06.30		eddy reconstruction, surface data supplementation
SSS	salinity	1993.01.01-2024.12.31, 2024.01.01-2025.06.30		eddy reconstruction, surface data supplementation
SLA	sea level anomaly	1993.01.01-2024.12.31		eddy reconstruction
surface current	u and v	2024.01.01-2025.06.30		eddy detection

The Argo dataset is provided by China Argo Real-time data center (CARDC, https://www.argo.org.cn), and these data were collected and made freely available by the International Argo Programme and the national programs that contribute to it (https://argo.ucsd.edu, https://www.oceanops.org). The Argo Programme is part of the Global Ocean Observing System. All the Argo temperature and salinity profiles have been post-quality-controlled by CARDC (Liu et al., 2021). The GTSPP temperature and salinity profiles are sourced from the National Centers for Environmental Information (NCEI) of National Oceanic and Atmospheric Administration (NOAA) (https://www.ncei.noaa.gov/products/global-temperature-and-salinity -profile-programme). They are archived into monthly folders, with a temporal resolution of daily observations and spatially distributed as discrete point measurements. The in-situ observations of WOD are also from NCEI/NOAA (https://www.ncei.noaa.gov/access/world-ocean-database). They are archived into folders by year, with one folder per year. These profiles have been quality controlled mainly including monotonicity check, domain and spike detection, and temperature-salinity gradient tests. There are 12,648 Argo profiles in total, 5,461 profiles of GTSPP, and 7,129 from WOD ranging from 15 °N to 35 °N and 114 °E to 135 °E during the period from January 1, 2024 to June 30, 2025.

The Group for High Resolution Sea Surface Temperature (GHRSST) product is provided by CMEMS (Copernicus Marine Service，https://podaac. jpl. nasa. gov/dataset/MUR-JPL-L4-GLOB-v4.1). This daily product integrates infrared and microwave observations with a pixel resolution of 0.01 °. The daily SSS product is from SMAP (Soil Moisture Active and Passive, https://data.remss.com/smap/SSS/V06.0/FINAL/L3/). The SSS data is resampled onto a 0.25° fixed grid using the Backus-Gilbert optimal interpolation (Chaubell et al., 2017) from the 70 km orbital data, forming a daily

https://doi.org/10.5194/essd-2026-398
Preprint. Discussion started: 11 June 2026

averaged Level 3 salinity product dataset. The selected SST and SSS data from January 1, 2024, to June 30, 2025 cover the area from 15 °N to 35 °N and 114 °E to 135 °E.

The satellite altimeter data used to detect the mesoscale eddies is the gridded products obtained with Multiscale Interpolation Ocean Science Topography (MIOST) from the AVISO (Archiving, Validation, and Interpretation of Satellite Oceanography, https://www.aviso.altimetry.fr/en/data/products/sea-surface-height- products/). Two daily products with a pixel resolution of 0.125 ° are used in this study which include longitude, latitude, time, SSH, and sea surface velocity. The selected satellite data from January 1, 2024, to June 30, 2025 covers the area from 15 °N to 35 °N and 114 °E to 135 °E. These data were processed by Data Unification and Altimeter Combination System (SSALTO/DUACS) and distributed by AVISO with support from CNES (Centre National d'Etudes Spatiales).

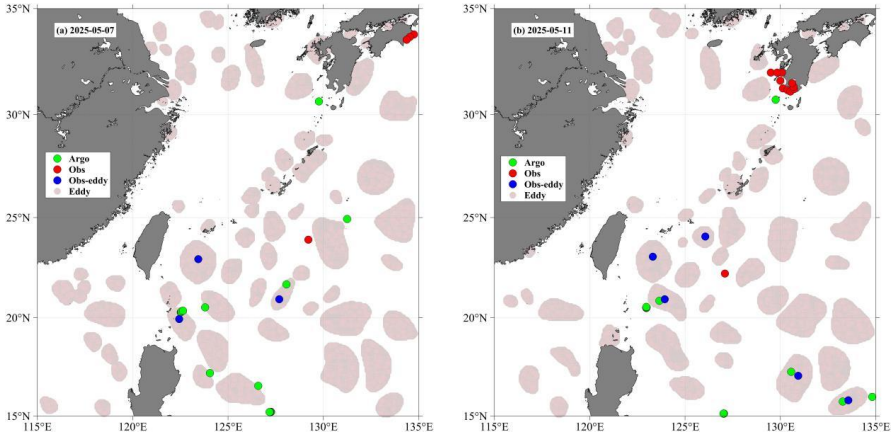

Figure1. Distribution and quantity statistics of observational data on May 7 (a) and 11 (b), 2025. The green circle is Argo profiles used for data fusion. The red circle indicates the historical observations from GTSPP and WOD. The bule circle is the Argo profiles used for eddy reconstruction. The pink dots are reconstructed eddy profiles.

2.2 Reconstruction of mesoscale eddy

A method for reconstructing the three-dimensional structure of eddies enhanced by in-situ observations is adopted. This method combines in-situ measurements within eddies with an improved density reconstruction algorithm based on a universal mesoscale eddy structural model (Wang et al., 2025). Based on the universal structure of mesoscale eddies, the three-dimensional density structure of eddies is reconstructed by satellite and Argo observations. Building upon this reconstructed density field, a machine learning–based temperature-salinity (T–S) profile reconstruction model is developed. The reconstructed eddy density profiles, along with eddy elements (polarity, eddy center, and radius) and sea surface elements (temperature, salinity, and dynamic height), serve as input data in the data-driven machine learning model to reconstruct the temperature and salinity structure of the eddies. By enhancing the representation of vertical stratification within mesoscale eddies, this method retrieves both their geometric characteristics (polarity, center location, and radius) and their internal properties, such as temperature and salinity. The reconstructed T–S profiles serve as high-resolution supplementary data within eddy regions and are subsequently used in multi-source data fusion analyses. As shown in Fig. 1, the number of reconstructed eddies on May 7 and 11, 2025 are 71 and 61 with 12,341 and 11,762 internal temperature and salinity profiles (the pink dots in Fig. 1), respectively. Each day, more than ten in-situ observations are sparsely distributed across the study region.

https://doi.org/10.5194/essd-2026-398
Preprint. Discussion started: 11 June 2026

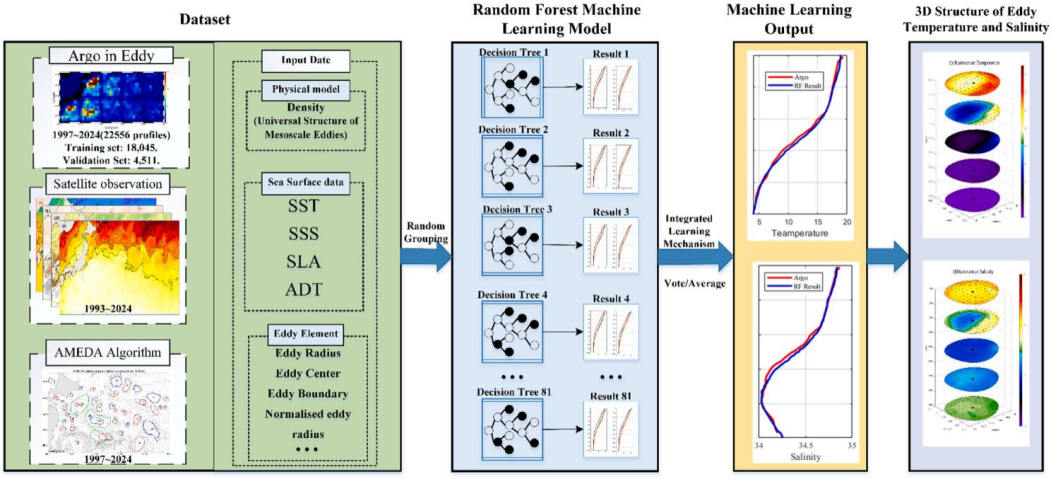

Figure 2. Random forest machine learning modeling.

2.3 Gradient-dependent Optimal Interpolation

The data fusion algorithm used in this paper, named gradient-dependent optimal interpolation, is an improved Optimal Interpolation (OI) based on the gradient-dependent correlation scale (Zhang et al., 2013; 2020; 2021). On the basis of least-squares theory, it improves the background error correlation scale model by incorporating diffusion principles. The analysis value at each grid point is obtained by adding the background value to an observation increment weighted by optimal weights. The standard equation of the influence of M observations on the analysis point is given in Eq. (1). A critical part of the scheme involves estimating the optimal weights. According to minimum variance theory, the optimal weight can be determined by solving Eq. (2)(Gandin, 1963). Shown as in Fig. 3, the observation data are automatically adjusted according to different regions of the eddy using gradient-dependent optimal interpolation. Inside the eddy, reconstructed eddy profiles serve as the primary data source, supplemented by observations. At the eddy edges, the background field, observations, and reconstructed profiles are combined using optimal weights. Outside the eddy, the background field is dominant, with observations providing supplementary information.

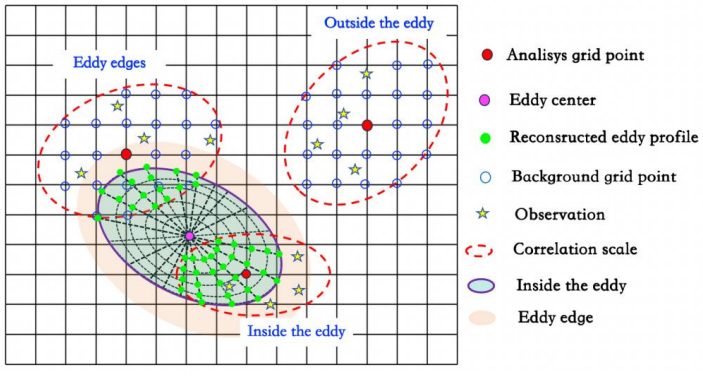

Figure3. Principles of multi-source data fusion by gradient-dependent optimal interpolation.

$$v_i^a = v_i^b + \sum_j^M \omega_{ij} \delta y_j^0 \quad (1)$$

https://doi.org/10.5194/essd-2026-398
Preprint. Discussion started: 11 June 2026

Open Access Earth System Science Data Discussions

$$\sum_{j=1}^{M} \omega_{ij}\mu_{jk} + \eta_k\omega_{ik} = \mu_{ik}, \quad k=1,\ldots,M \tag{2}$$

where v_i^a is the analysis value and v can be any environmental variable, such as temperature or salinity. The v_i^b, given by the daily background, is the first estimated value. The subscript i denotes the number of gridded points used for analysis, and j and k denote the number of available sites of observations. For observational increments, $\delta y_j^0 = y_j^0 - H(v_j^b)$, the observational operator H is used to convert the background into the first guess of the observation y_j^0. A radial distance is set to ensure that only observations located within a specified range surrounding each analysis point are used. Each increment has an optimal weight w_{ik} associated with the background error correlations μ_{jk} and μ_{ik}. Here, μ_{jk} is the background error correlation between two oservation points j and k, while μ_{ik} is the correlation between the analysis point i and the observation point k. The parameter η_k, often set to be a constant η (its value will be detailed in Sect. 3.1), is the square of relative observational errors compared with the background errors.

The correlations are usually assumed to follow a Gaussian exponential function, and are inversely proportional to the distance (Kalnay 2003; Zhang et al., 2021, 2022), as shown in Eqs. (3) and (4):

$$\mu_{ik} \sim \exp\left[-\frac{(x_i-x_k)^2}{(L_\emptyset/G_x)^2} - \frac{(y_i-y_k)^2}{(L_\emptyset/G_y)^2}\right] \tag{3}$$

$$G_x = 1 + \frac{|\partial v/\partial x|}{E(|\partial v/\partial x|)}, \quad G_y = 1 + \frac{|\partial v/\partial y|}{E(|\partial v/\partial y|)} \tag{4}$$

where x and y are the longitude and latitude, respectively, and $L_\emptyset/G$ depends on the Rossby radius of deformation and changes in the horizontal gradient that define the scale of correlation of the background error. The parameter $L_\emptyset$ is the correlation scale obtained from the product of the scale parameter L and the cosine function of the latitude $\emptyset$ at the analysis gridded point. The parameter G_x and G_y, calculated by daily background data, is associated with the horizontal gradient at location i. The scale parameter L and radial distance R are also related to the observations involved in the fusion. When R is equal to 1°, the observations are significantly correlated with the analysis grid points. And more than half of the analysis grid points exhibit high correlation with $L \geq 3°$ (Fig. 3).

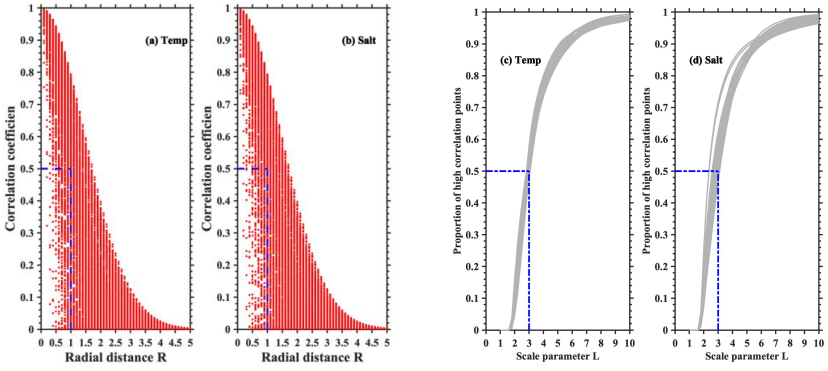

Figure4. Statistic of temperature and salinity correlation coefficients for the radial distance R (a, b) and scale parameter L (c, d). The high correlation indicates the correlation coefficient exceeding 0.5.

3. Results

3.1 Procedure and Parameters of Data Fusion

Employing the methodology outlined in Sect. 2.2, temperature and salinity profiles inside mesoscale eddies are reconstructed. These profiles are then fused with multi-source observational data using Gradient-dependent optimal

https://doi.org/10.5194/essd-2026-398
Preprint. Discussion started: 11 June 2026

interpolation (OI) to generate a high-resolution regional fusion dataset EFGO (Eddy Model Fusion Gradient Optimal Interpolation Data) (Fig. 5). Data fusion modeling primarily involves steps such as the standardization of observations, construction of background, and correlation scale calculation. EFGO covers the region from 15°N to 35°N and 115°E to 135°E, spanning the period from January 1, 2024, to June 30, 2025. It features a spatial resolution of 1/16°, a temporal resolution of one day, and comprises 44 unevenly spaced vertical layers. EFGO comprises temperature, salinity, surface sound channel depth (SCD), and thermocline parameters (mixed layer depth (MLD), thermocline bottom depth (TBD) , and thermocline temperature gradient (TTG)). Additionally, it also includes eddy characteristic parameters, such as eddy center location, radius, type, boundary, and internal temperature-salinity profiles, comprising a total of 27 variables.

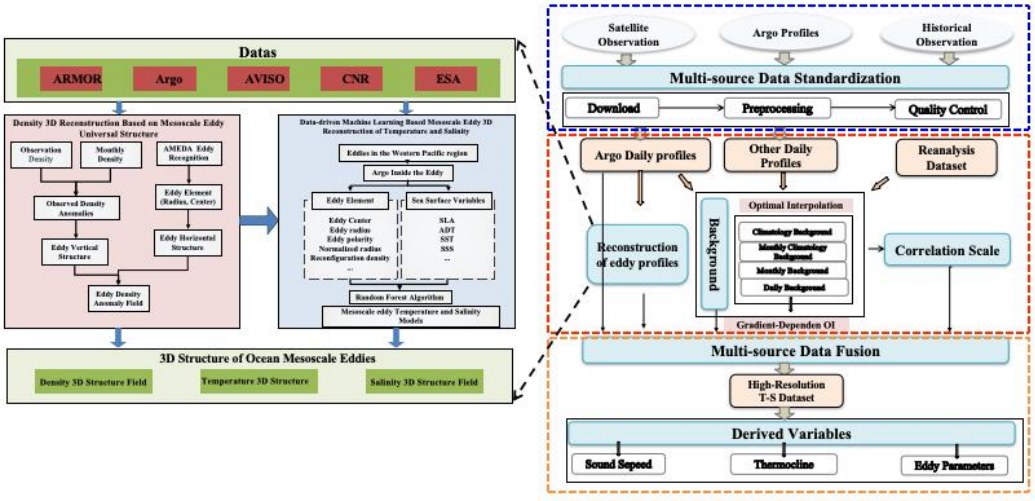

Figure 5. EFGO fusion dataset construction workflow.

In the Gradient-dependent optimal interpolation, the relative ratio of observation error to background error, denoted as η, plays a critical role in determining the fusion results. A smaller η facilitates more effective absorption of high-frequency signals from observations, whereas a larger η causes the analysis to converge closer to the background. However, a trade-off exists: an excessively small η may introduce spurious information, while an overly large η fails to adequately extract observational informationis. As a dimensionless factor, η typically ranges from 0.01 to 0.5 (Zhang et al., 2021). The optimal value needs further discussion to be determined by evaluating T/S differences between fusion results and in situ measurements. Figure 6 presents comparative results derived from varying η values by selecting four independent Argo profiles. These profiles were collected on May 7, 2025, at the edge of a warm-core eddy. When η is 0.01 to 0.5, the maximum temperature differences between the fusion results and observations do not exceed 1.5℃, with biases predominantly remaining below 1.0℃ within the upper 1000 m. Similarly, salinity biases peak at 0.15, mostly staying under 0.1. Notably, the magnitude of temperature and salinity biases does not exhibit a linear proportionality to η. In this study region, moderate η values (e.g.,η= 0.25) yield smaller *T/S* biases relative to the in situ profiles.

https://doi.org/10.5194/essd-2026-398
Preprint. Discussion started: 11 June 2026

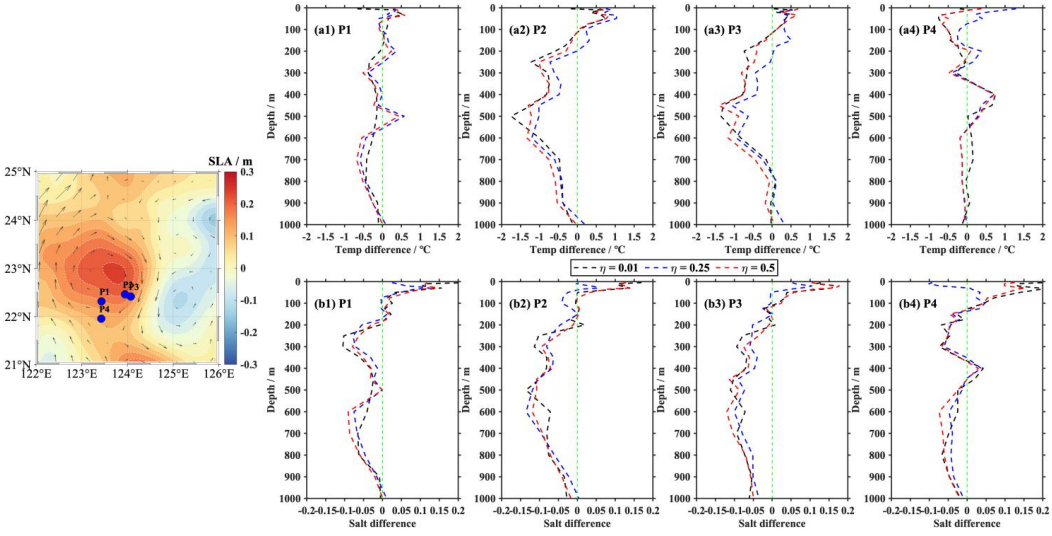

Figure 6. Temperature (a1-a4) and salinity (b1-b4) differences of fusion results for varying η relative to Argo observational profiles.

3.2 Verification of the High-resolution Dataset

3.2.1 Relative analysis error

The interpolation scheme provides an estimation of the relative analysis error given by $p_i = 1 - \sum_{k=1}^{M} w_{ik}\,\mu_{ik}$, where the analysis error is scaled by the background error variance. This parameter represents the percentage of the analysis error relative to the background error, thereby characterizing the correction accuracy of data fusion. Figure 7 displays the mean temperature analysis errors within the depth 0-1000m on the 15th of each month in 2024. It is evident that these errors are no more than 0.50 (i.e. half of the background error), which are equal to be the observation errors owing to the chosen value of $\eta = 0.25$ (Fig. 6) used in Eq. 2. In other words, the analysis results are close to the observations. The significant correction effects of the data fusion are manifested in regions characterized by mesoscale eddies. Analysis errors are significantly smaller (<0.1, representing less than one-tenth of the background error) in densely sampled observation areas. Although analysis errors increase in data-sparse marginal areas, the maximum mean relative analysis error does not exceed 0.5.

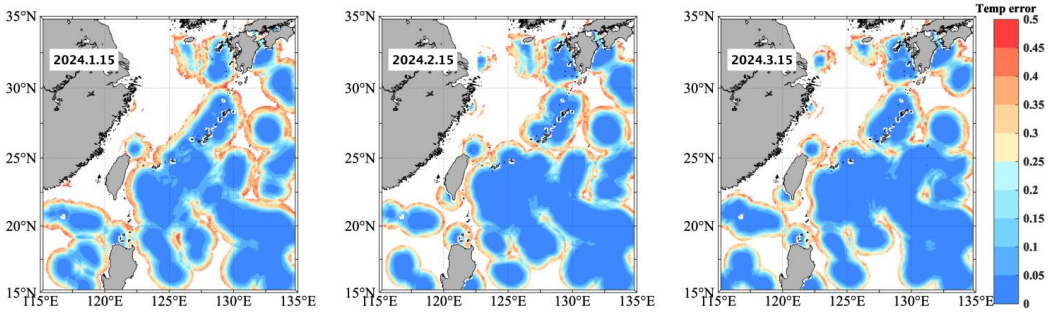

https://doi.org/10.5194/essd-2026-398
Preprint. Discussion started: 11 June 2026

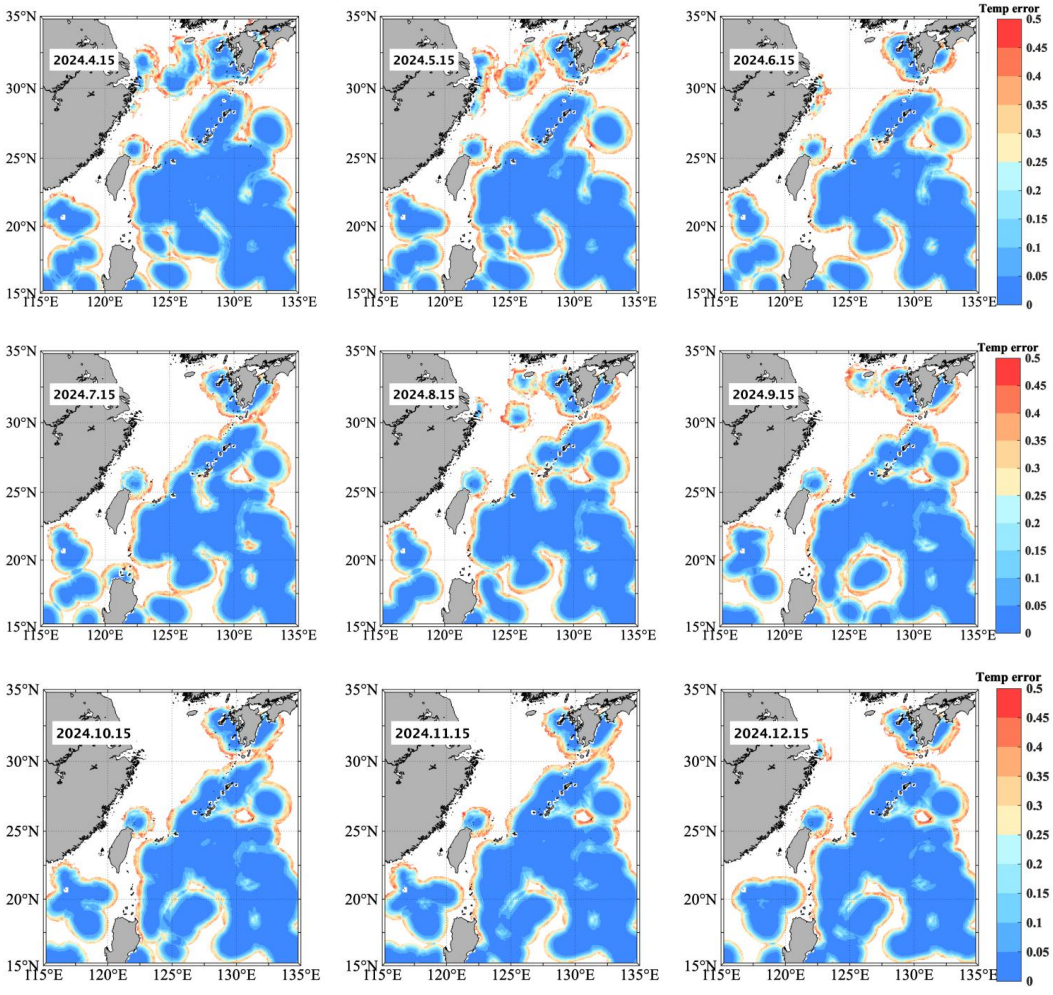

Figure 7. Maps of vertically mean (0–1000 m) temperature analysis errors for the 2024 fused dataset. Blank regions denote areas where no observational correction was applied.

Statistics of relative analysis errors, categorized by error magnitude for different water layers, show that temperature and salinity share a similar pattern in the proportion of errors (Fig. 8). An inverse relationship is visible between error magnitude and frequency for both temperature and salinity. Only ~5% of grid points exhibit relative analysis errors > 0.5. In contrast, ~70% of grid points across all depths have errors < 0.1, while the remaining ~30% exceed this threshold. Specifically, the error distribution is as follows: 12% in the 0.1–0.2 range, 8% in 0.2–0.3, 5% in 0.3–0.4, and ~5% > 0.4. With increasing depth, these proportional distributions show minimal variation, fluctuating by only 1–2% across different magnitude bins.

https://doi.org/10.5194/essd-2026-398
Preprint. Discussion started: 11 June 2026

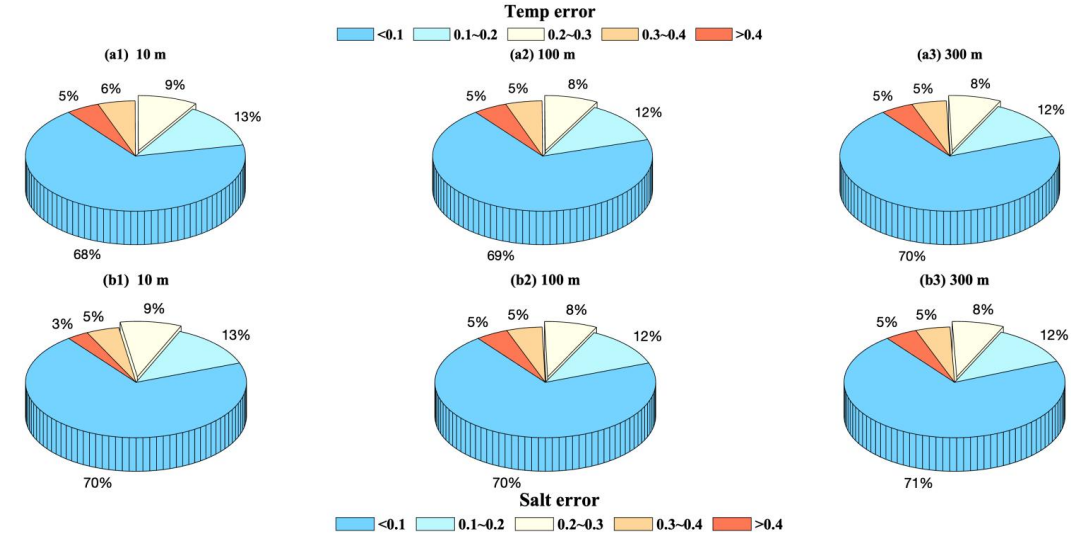

Figure 8. Statistics of the mean relative analysis errors for temperature (a1-a3) and salinity (b1-b3) at various depths from January 1, 2024, to June 30, 2025.

3.2.2 Two-dimensional spectral analysis

Two-dimensional spectra, utilizing Fast Fourier Transform (FFT) and ideal high-pass filtering, can evaluate the capability of oceanographic data products to extract high-frequency oceanic signals. Taking the 10-m temperature and salinity anomaly on May 12, 17, and 22, 2025, as examples, Figures 9 and 10 present a comparative extraction of meso- and small-scale signals retained in data from GLORYS12, EFGO, and HYCOM. In this process, the temperature and salinity are first transformed into the frequency domain via Fourier Transform to extract spectral information. Subsequently, an ideal high-pass filter was applied to remove low-frequency signals with wavelengths exceeding 40 grid steps. Finally, the filtered temperature and salinity anomaly are reconstructed through an Inverse Fourier Transform. The spatial continuity of the anomaly contours is inversely proportional to the frequency of the temperature and salinity variations.

Three kinds of data products reveal similar spatial patterns of temperature anomalies: negative anomalies predominate in the South China Sea, the East China Sea, and the areas between 20-30°N east of 130°E, whereas positive anomalies dominate the open ocean between 120-130°E. However, GLORYS12 exhibits relatively smooth contours and the largest extremes in temperature anomalies, reflecting temperature variations driven primarily by large-scale circulation patterns. In contrast, EFGO provides a more refined representation of mesoscale processes, while HYCOM captures distinct dynamic features along boundaries, including land-sea interfaces and shear zones associated with dynamic processes. Due to its 3-hour temporal resolution, HYCOM displays more small-scale variations in temperature anomalies. And the positive or negative anomalies are spatially concentrated in HYCOM. EFGO and GLORYS12 exhibit a spatial pattern characterized by alternating positive and negative temperature anomalies. By comparison, EFGO gives a greater abundance of mesoscale positive and negative anomaly distributions compared to GLORYS12 from May 12 to May 22. This distinction was particularly evident on May 22: while GLORYS12 displays a large-scale, adjacent positive-negative anomaly structure near 130°E, 23°N, EFGO features multiple negative anomaly structures in the north surrounding a southern positive anomaly center.

https://doi.org/10.5194/essd-2026-398
Preprint. Discussion started: 11 June 2026

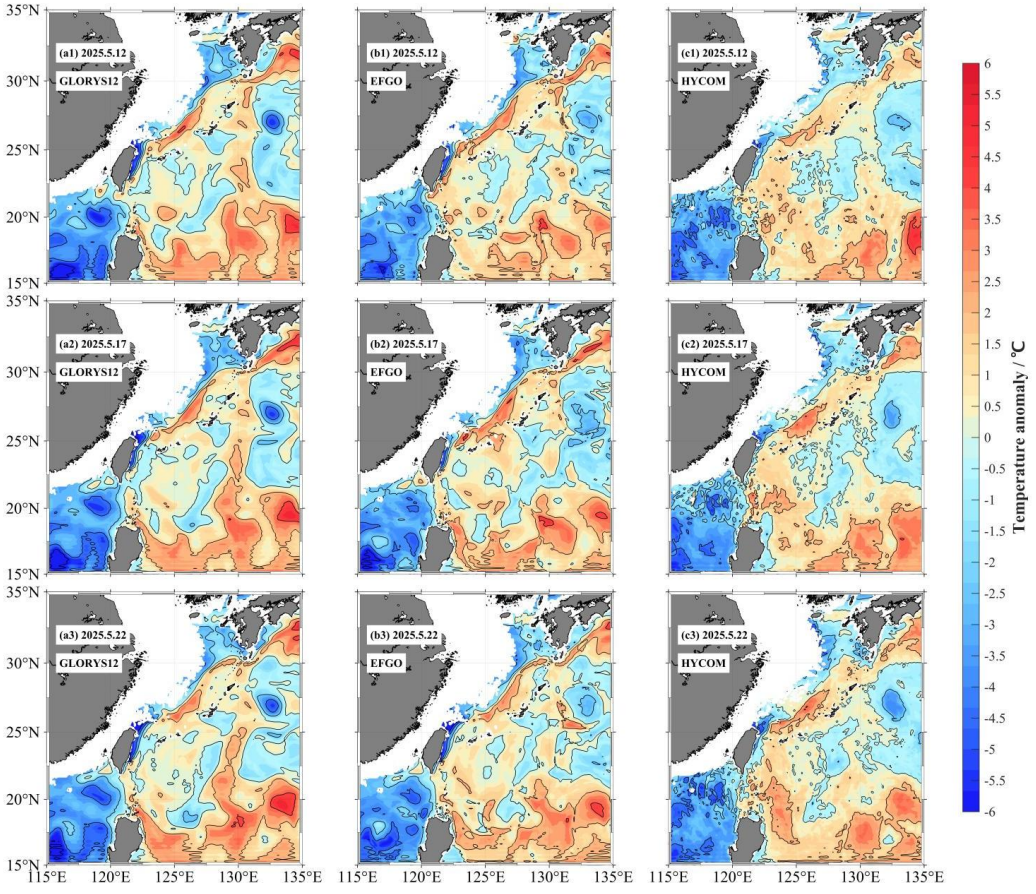

Figure 9. Comparison of two-dimensional spectral analysis results for temperature across different data products.

Across the three datasets, salinity generally exhibits a distribution trend of negative anomalies in the west and positive anomalies in the east. Similar to temperature, GLORYS12 clearly reflects large- and meso-scale salinity variations, while EFGO captures more mesoscale features. In contrast, HYCOM salinity anomalies contain abundant small-scale information, which is particularly pronounced along boundaries, whereas the anomalies in open waters remain relatively uniform. EFGO exhibits more detailed salinity variations than GLORYS12, yet it excludes numerous small-scale fluctuations (associated with hourly resolution) seen in HYCOM. For instance, on May 22, EFGO exhibits a detailed structure of a negative anomaly center at 125°E, 17°N.

https://doi.org/10.5194/essd-2026-398
Preprint. Discussion started: 11 June 2026

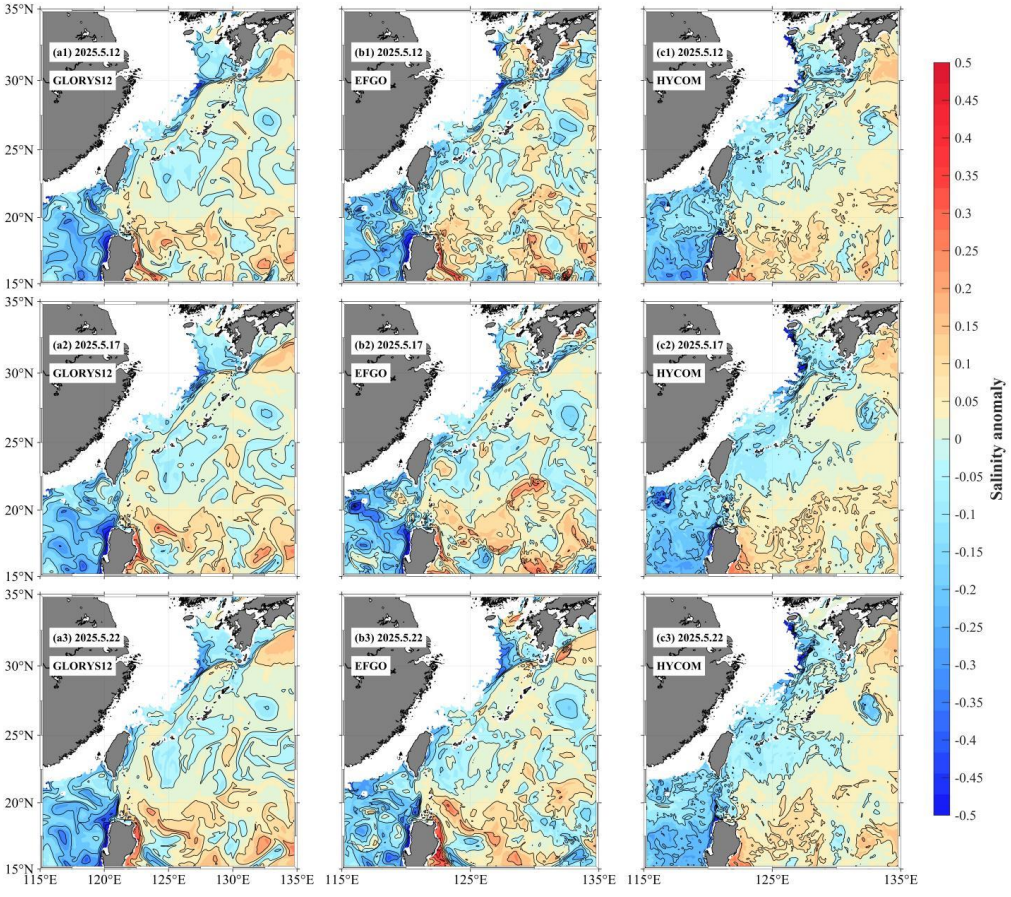

Figure 10. Same as Fig. 9, but for salinity.

3.2.3 Comparison with observations

Taking into account the spatial distribution of stations, observation time and depth, as well as the completeness of temperature and salinity profiles, ten Argo profiles are collected between January 1, 2024, and June 30, 2025 (Fig. 11a). Specifically, data are selected at one-month intervals within a three-day window before and after the 15th of the month, requiring a maximal profiling depth greater than 500 m. As shown in Fig. 11b, a meridional transect along 131°E from WOD (S02, observed from September 7, 2024, to September 25, 2024) and a zonal section from Argo (S01, from January 19, 2025, to March 3, 2025) are also selected to compare the temperature and salinity results derived from the EFGO, GLORYS12, and HYCOM datasets.

In terms of temperature profile distribution (Fig. 12a), all three data products show good consistency with the Argo observations. Below 400 m, the temperature biases for all datasets are generally less than 0.5℃. Around 200 m, where temperature gradients are sharp, the biases are relatively larger, but the maximum bias does not exceed ± 2℃. In comparison, EFGO exhibits the smallest temperature bias against observations across nine of the ten profiles (excluding station P09), followed by GLORYS12, with HYCOM showing the largest bias. At station P09, all three datasets align closely with the Argo observations (maximum bias < 1℃). HYCOM shows a smaller bias, while the vertical variations in bias for EFGO and GLORYS12 are more consistent.

https://doi.org/10.5194/essd-2026-398
Preprint. Discussion started: 11 June 2026

The comparison results for salinity profiles are relatively complex (Fig. 12b). From top to bottom, salinity bias exhibits a trend of initially increasing, then decreasing, and finally increasing again. All datasets capture this same trend as the observed profiles, while the salinity biases vary across different depths. For profiles P01, P04, P05, P08, and P10, EFGO shows remarkable consistency with Argo observations within the top 1000 m, with salinity biases less than ±0.05. In these profiles, GLORYS12 biases range from approximately -0.05 to 0.1, while HYCOM biases are around ±0.1. For profiles P02, P03, and P06, EFGO aligns closely with observations between 100 and 600 m, though biases are slightly larger (> ±0.1) in the near-surface layer and below 800 m. GLORYS12 exhibits a pattern similar to EFGO, whereas HYCOM shows larger biases in the same layers across these profiles. At station P07, differences are primarily confined to the top 100 m; EFGO and GLORYS12 have maximum biases of approximately ±0.2, while HYCOM exceeds 0.2. Finally, at station P09, maximum biases are concentrated between 200 and 500 m. In comparison, EFGO performs best (< ±0.1), followed by GLORYS12, with HYCOM showing the largest biases.

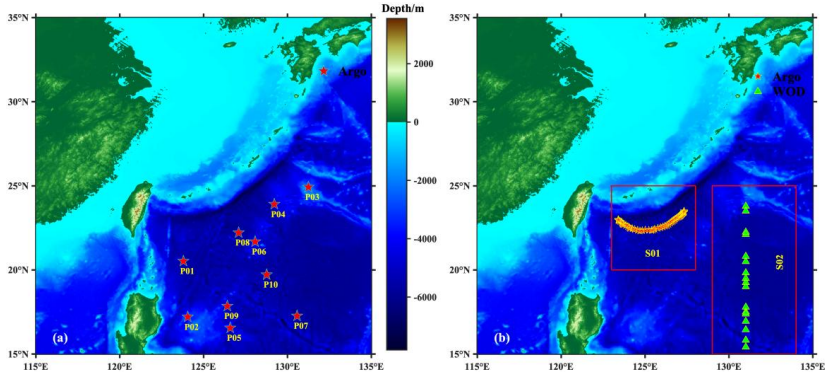

Figure 11. Argo profiles (a) and observation sections (b) for in-situ validation.

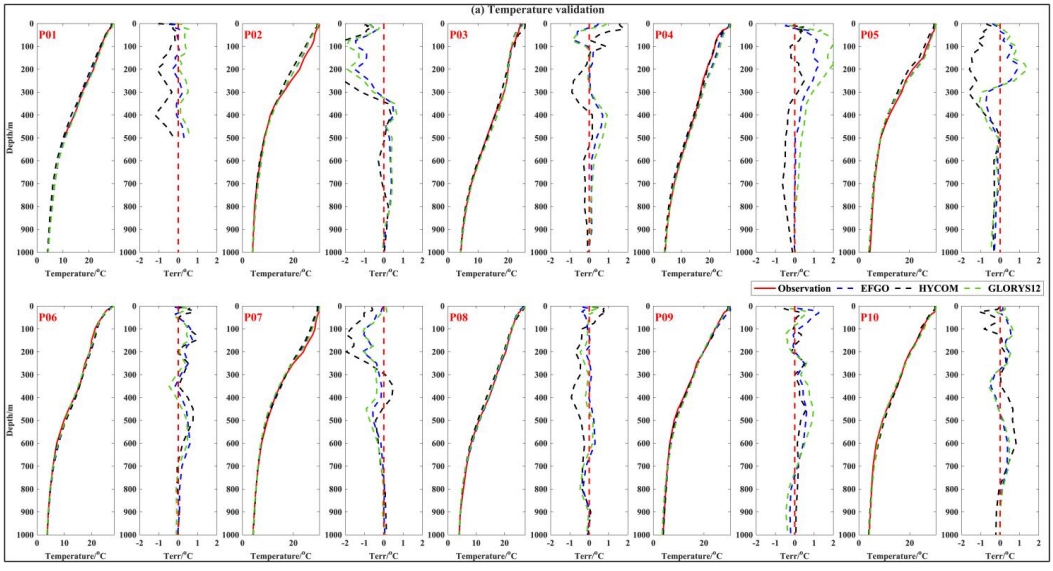

https://doi.org/10.5194/essd-2026-398
Preprint. Discussion started: 11 June 2026

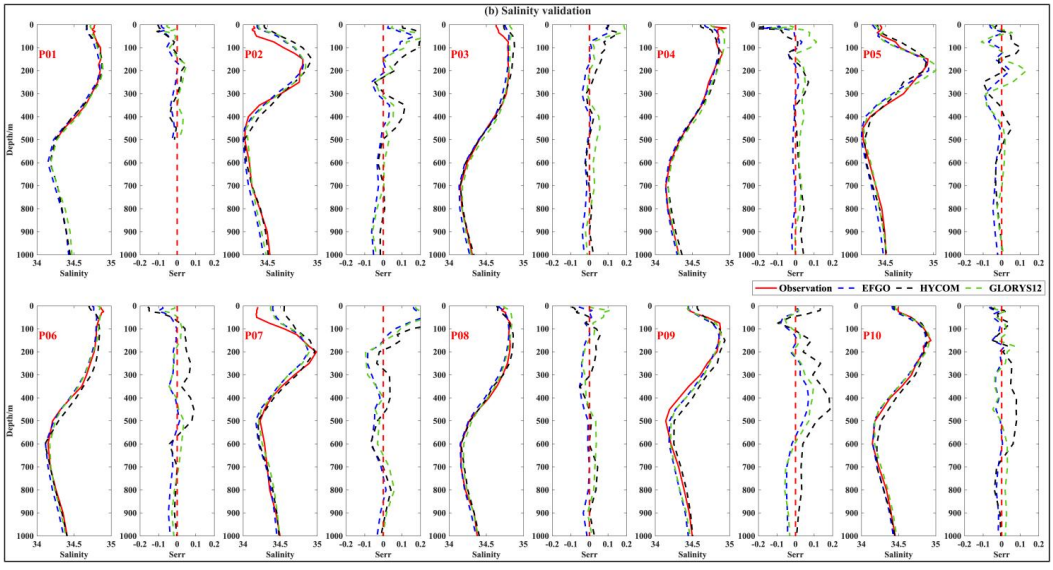

Figure 12. Temperatute (a) and Salinity (b) profiles and bias curves against Argo observations for various data products at each station.

Along the Argo zonal section (S01), the sinking and fluctuating features of EFGO temperature isolines with longitude closely resemble those of the observed section (Fig. 13a). HYCOM exhibits patterns similar to EFGO, whereas the GLORYS12 isolines appear relatively smooth, showing little zonal (east-west) variation. Correspondingly, EFGO yields the smallest temperature bias against Argo observations, remaining within ±0.25℃ across the entire section. The temperature biases of GLORYS12 exceed ±0.5℃ (up to ±0.75℃) at specific observation points around 150 m depth. In contrast, HYCOM temperatures are generally lower than the Argo observations, with most biases ranging between -1.5℃ and 0.25℃. Similar to temperature, EFGO salinity patterns align most closely with the observed section (Fig. 13b): salinity is relatively uniform within the top 200 m (approx. 34.7–35.0), exhibiting varying degrees of fluctuation from west to east, with significant sinking of salinity isolines observed at the station near 125.5°E. In contrast, GLORYS12 shows smaller zonal variations in salinity isolines, while HYCOM presents outliers at certain locations (e.g., below 300 m at 126.25°E). Regarding accuracy, EFGO salinity biases remain within ±0.05. GLORYS12 exhibits higher salinity than observations within the top 200 m, whereas HYCOM biases range from -0.15 to 0.1, predominantly showing negative values.

As shown in Fig. 13c, along the WOD observation transect (S02), the temperature variations with depth and latitude across all datasets generally resemble the observed patterns. However, EFGO aligns more closely with the observations, particularly regarding the sinking of temperature isolines with latitude between 200 and 500 m. The warm layer thickness (above the 23.5℃ isotherm) in the top 200 m for GLORYS12 is relatively larger compared to other datasets, whereas the warm layer in HYCOM is thinner. Correspondingly, GLORYS12 temperature biases exceed ±1.0℃ in some areas, with predominantly positive biases south of 20°N and above 200 m. HYCOM temperatures are significantly lower than observations in the top 400 m, with most biases exceeding -1.5℃ (in magnitude). In contrast, EFGO matches the observations best, with temperature biases remaining within ±0.5℃ across the entire section. A high-salinity core is present above 100–200 m on this section, while a significant southward intrusion of low-salinity water occurs between 400 and 800 m. It is a feature clearly captured by all datasets (Fig. 13d). However, all three data products generally exhibit higher salinity values than the WOD observations. EFGO yields the smallest salinity bias

https://doi.org/10.5194/essd-2026-398
Preprint. Discussion started: 11 June 2026

Open Access Earth System Science Data Discussions

330 (approx. ±0.05), followed by GLORYS12, with most biases within ±0.1, whereas HYCOM biases frequently exceed ±0.15.

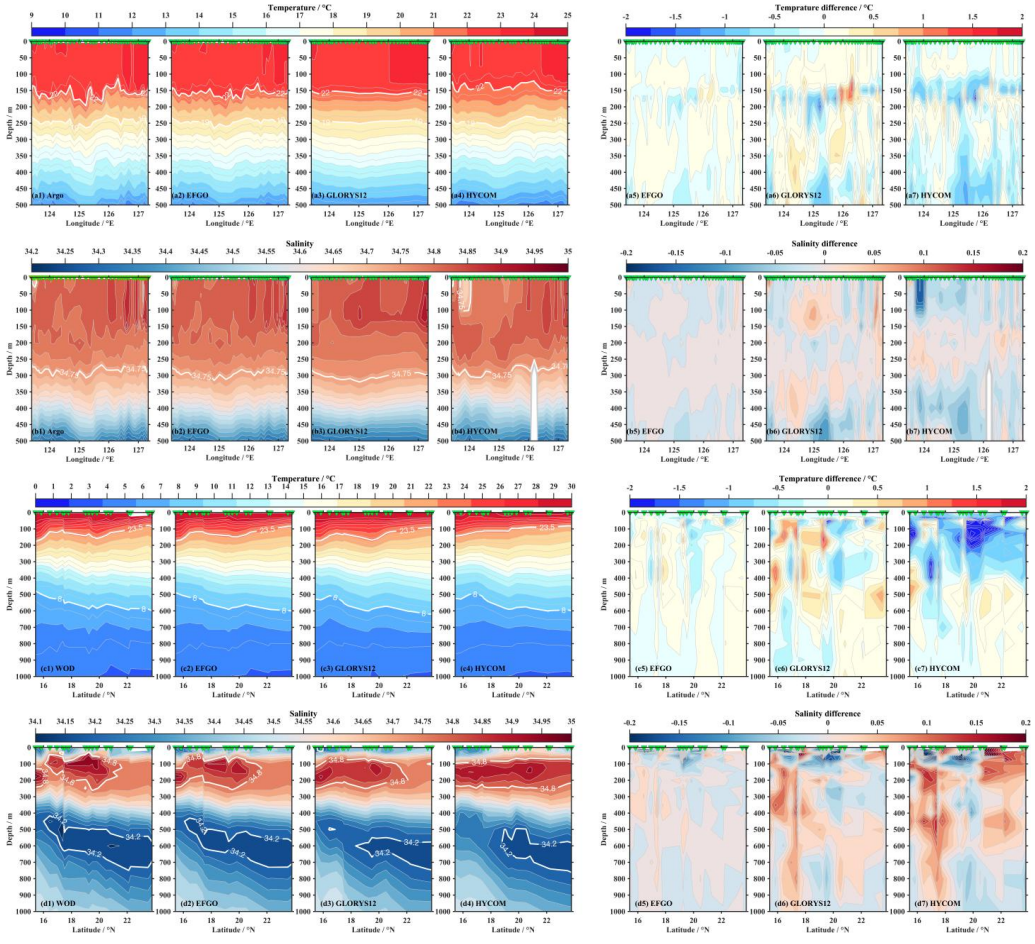

335 **Figure 13.** Temperature (a1-a4; c1-c4) and salinity (b1-b4; d1-d4) sections and corresponding bias (5-7 subplots) against Argo or WOD observations for various data products along S01 and S02. The green triangles indicate the observation locations.

4. Discussion

4.1 Eddy model and data fusion

340 Combining physical process models with data-driven machine learning provides effective results in oceanic mesoscale 3D structure reconstruction. The boundaries of mesoscale eddies serve as a delineating factor. In the context of observed profiles utilized for reconstruction, proximity to the eddy center and the presence of a stronger geostrophic balance (i.e., a reduced Rossby number) have been observed to yield more precise reconstructions (Wang et al., 2025). Conversely, profiles positioned outside the mesoscale eddy's boundaries do not align with the conditions stipulated by the unified 345 structure theorem for mesoscale eddies. Consequently, they are deemed inadequate for effective mesoscale eddy reconstruction.

https://doi.org/10.5194/essd-2026-398
Preprint. Discussion started: 11 June 2026

Open Access Earth System Science Data Discussions

As shown in Fig. 14, for the cold-core eddy located within 148 – 151° E and 32.5 – 35.5° N on June 15, 2019, the machine learning model was only capable of providing the three-dimensional structure within the mean eddy radius. Within this radius, the reconstructed temperature section shows good agreement with in-situ observations, particularly regarding the trend of cold water upwelling near the eddy center. The data fusion results EFGO preserve the combined information of observation and reconstructed structures, exhibiting a significant cold water upwelling trend at the eddy center (indicated by the 5℃ isotherm). Due to the constraints of the weighted average algorithm, EFGO displays smoother temperature contours. Multi-source information fusion is evident in the near-surface layer at 100 m, where the 15℃ isotherm was positioned deeper than in both the observation and reconstructed results. Nevertheless, EFGO ensures the continuity of the meridional temperature variation.

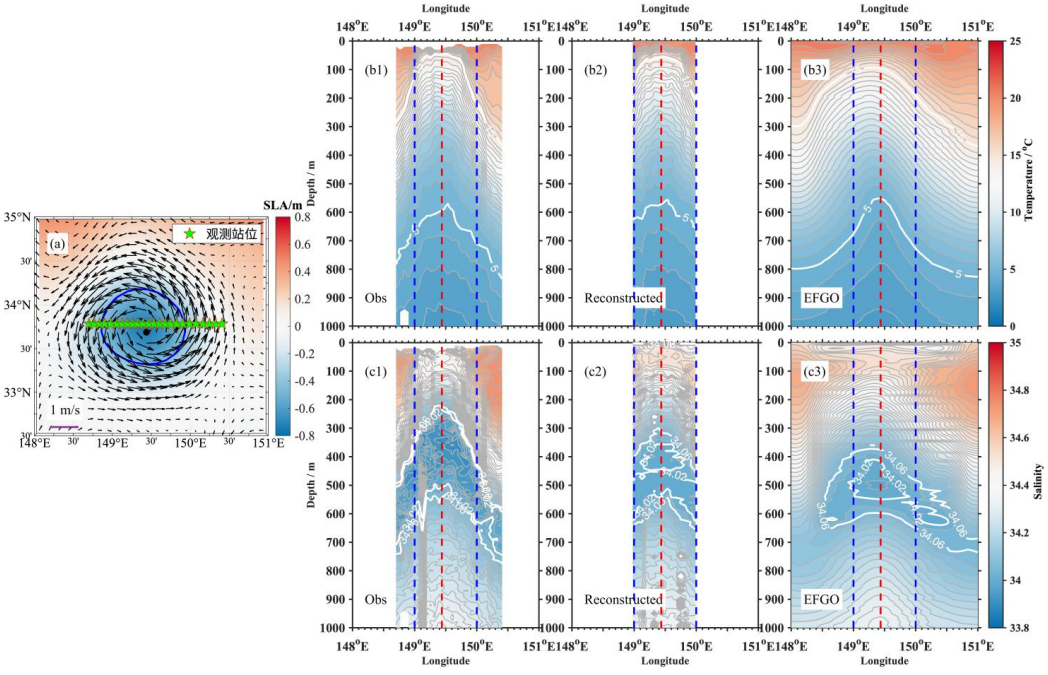

Figure 14. Comparison of temperature and salinity sections in a typical eddy region (a). (b1)-(b3) display the temperature section for observation, reconstructed eddy, and data fusion. (c1)-(c3) are the same but for the salinity. The blue solid line in (a) and blue dashed lines in (b-c) denote the eddy mean radius. The black dot in (a) and red dashed lines in (b-c) denote the eddy centers.

The observed salinity section exhibits significant small-scale fluctuations, with a low-salinity core in the eddy region between 250 and 500 m showing salinity values lower than 34.0. The reconstructed salinity shows good consistency with the in-situ data. Its low-salinity core sinks slightly, forming a closed loop between 300 and 500 m at the eddy center, with a corresponding slight increase in salinity. EFGO fuses the salinity characteristics of both observation and the reconstructed eddy. The salinity contours are smooth. The low-salinity core is located approximately between 300 and 600 m, and distinct low-salinity water masses are also present at the eddy boundaries. Although artificial intelligence can rapidly reconstruct the interior three-dimensional structure of the eddy, its algorithmic limitations at the eddy boundary necessitate the fusion of multi-source data to provide a more comprehensive view of the eddy periphery.

4.2 Potential application advantage

The eddy model, which is based on machine learning with physical constraints and observation enhancement, efficiently reconstructs temperature and salinity profiles within eddy. These reconstructed profiles serve as the primary data source

https://doi.org/10.5194/essd-2026-398
Preprint. Discussion started: 11 June 2026

for data fusion. With a daily average of over 40 eddies and more than 10,000 reconstructed profiles, this densely distributed data makes it possible to achieve fusion products with a resolution of daily and 1/16°. Consequently, the primary potential advantage of EFGO lies in the accurate reproduction of the dynamic structures of mesoscale processes. Taking the anticyclonic eddy located between 122° E – 125° E, 22° N – 24° N and the cyclonic eddy between 131° E – 134.5° E, 25.5° N – 28.5° N as examples (Fig. 15), Figure 16 compares the similarities and differences in the eddy structure presented by EFGO, GLORYS12, and HYCOM at the same time point (May 9, 2025).

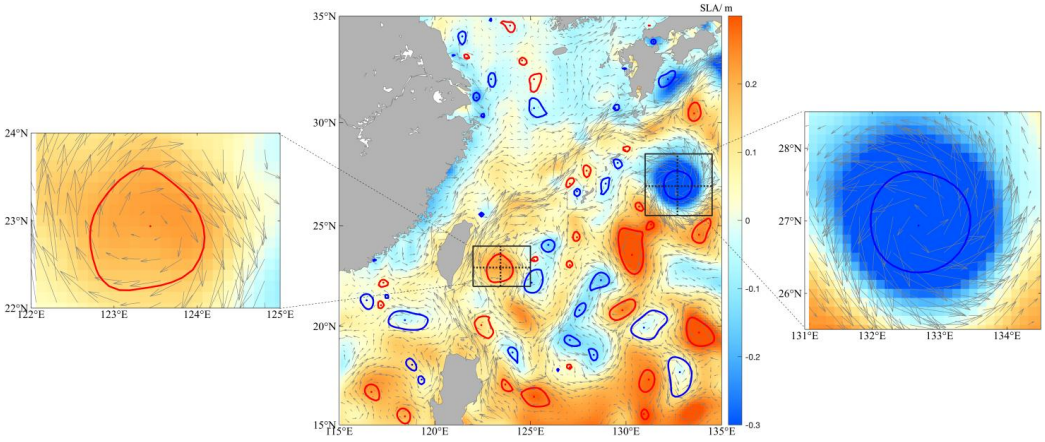

Figure 15. Sea Surface Level Anomaly (SLA), sea surface current, and mesoscale eddies on May 9, 2025, along with the locations of typical cyclonic and anticyclonic eddies.

As shown in Figs. 16 (a1)-(c1), all three datasets demonstrate the homogeneity of water masses within the typical anticyclonic eddy region. In comparison, the density contours in the fused data EFGO are more closed, with sharper water mass boundaries. Furthermore, the low-density center at the eddy core shown by EFGO aligns well with surface satellite observations. GLORYS12 exhibits strong homogeneity at the eddy core. However, its contours generally run parallel to the meridians, and the density gradients inside and outside the eddy are smaller, resulting in less distinct water mass characteristics. HYCOM also displays relatively distinct closed density contours, but there are noticeable small-scale fluctuations within the contours, which are related to its 3-hour temporal resolution. Below 600 m, the density gradient in HYCOM decreases significantly within the eddy, and the eddy features become less distinct.

In the cyclonic eddy region, the density contours in all three datasets are significantly closed, with distinct eddy boundaries. The density results from GLORYS12 exhibit strong homogeneity at the eddy core, with more regular and smoother contours (Fig. 16 (b2)). Due to its temporal resolution, HYCOM shows noticeable small-scale fluctuations in its density contours (Fig. 16 (c2)). In contrast, the EFGO results comprehensively present the characteristics of both GLORYS12 and HYCOM (Fig. 16 (a2)). Its density contours display distinct and regular closed features, revealing more detailed density variations than GLORYS12. For instance, the density gradients at the eddy core between 200–500 m depth are more pronounced, indicating that EFGO is capable of more fully representing meso- and sub-mesoscale features with daily temporal resolution.

Certainly, beyond eddy enhancement, EFGO can also provide environmental parameters with high spatiotemporal resolution, such as thermocline parameters and sound channel depth. This highlights its potential value for applications in marine scientific research or underwater acoustics.

https://doi.org/10.5194/essd-2026-398
Preprint. Discussion started: 11 June 2026

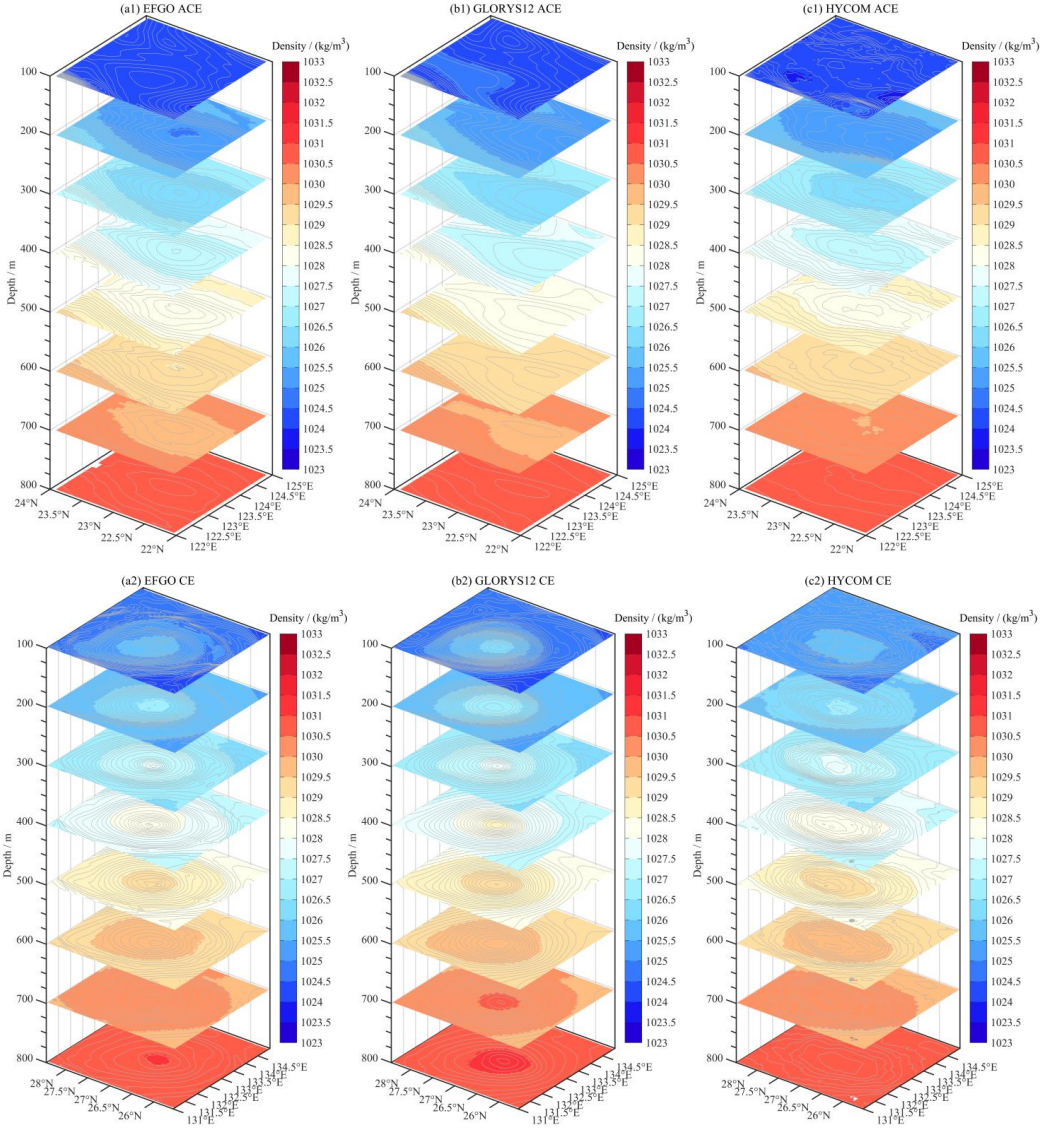

Figure 16. Three-dimensional structures of eddy density in typical anticyclonic (a1, b1, c1) and cyclonic (a2, b2, c2) on May 9, 2025, derived from EFGO (a), GLORYS12 (b), and HYCOM (c) datasets.

5. Data availability

The dataset of Eddy Model Fusion Gradient Optimal Interpolation Data (EFGO) generated in this study was deposited in Zenodo, whose DOI is https://doi.org/10.5281/zenodo.20396796（Zhang et al., 2026）. The dataset includes four files: “EFGO Data Reading and Plotting.zip”, “EFGO_202401-202412.zip”, “EFGO_202501-202506.zip”, and “Manual of EFGO.zip”.

https://doi.org/10.5194/essd-2026-398
Preprint. Discussion started: 11 June 2026

6. Conclusions

This study addresses the core challenge of high-resolution eddy modeling and data fusion in the Pacific western boundary current region. We constructed a novel data fusion framework based on gradient-dependent optimal interpolation and developed the EFGO dataset. This dataset features a daily temporal resolution and a spatial resolution of 1/16°, achieving the effective integration of multi-source observational data and reconstructed eddies. It incorporates seven data sources, including satellite remote sensing data, Argo T-S profiles, historical observations, and reconstructed eddy profiles. Specifically, temperature and salinity profiles within eddy were inverted using a machine learning model that combines data-driven approaches with physical constraints. The system fuses more than 40 reconstructed eddies and over 10,000 corresponding profiles daily.

During the data fusion process, the background error covariance is constrained by the horizontal gradients of marine elements, and the weights of different data sources are automatically fine-tuned based on their distance from the eddy center. This effectively reduces smoothing errors in strong gradient regions and significantly improves the fidelity of the dataset. The theoretical analysis error in the target region is less than 0.5 (half of the background error) and reach as low as <0.1 in eddy-rich or observation-dense regions. Approximately 70% of grid points exhibit errors less than 0.1 across all depths. Spectral analysis results indicate that, compared to GLORYS12 and HYCOM, EFGO is capable of presenting more refined features of mesoscale processes. Compared with Argo observation profiles, EFGO generally exhibits the smallest temperature (<0.5℃) and salinity (<±0.05) bias across the majority of profiles, followed by GLORYS12, while HYCOM shows the largest deviations. Along the observation section, EFGO aligns more closely with the observations, with most temperature bias within ±0.25℃ ~± 0.5℃and salinity bias less than ±0.05.

As an advanced and efficient technique for eddy reconstruction, machine learning has significantly improved the spatiotemporal resolution of the eddy region. This necessitates a theoretical data fusion approach, corrected by in-situ observations, to organically integrate large-scale background with these high-resolution mesoscale eddy dynamics. EFGO achieves spatiotemporal homogeneity and continuity in multi-scale environmental changes, while ensuring eddy reconstruction accuracy. A distinctive feature of this dataset is the enhanced reproduction of eddy characteristics, making it suitable for analyzing real-time eddy evolution and reflecting sub-mesoscale information. Furthermore, EFGO includes 27 environmental variables such as temperature, salinity, thermocline, surface layer sound channel, and eddy parameters. It shows great potential for various oceanographic applications. Due to computational constraints, this study focuses on regional modeling and data fusion. The applicability in global ocean requires further validation.

Author contributions

Chun Ling Zhang: Conceptualization, Methodology, Writing- Original draft preparation, Corresponding author.
Ao Ran Sun: Data curation, Writing- Original draft preparation.
Ke Feng Mao: Conceptualization, Reviewing and Editing, Co-corresponding author.
Zeng Hong Liu: Reviewing and Editing, Investigation, Co-corresponding author.
Peng Hao Wang: Methodology, Modeling test, Editing.
Li Fu Fu: Data curation, Methodology.
Yu Hang Zhu: Modeling test, Data curation.
Jia-Hui Fan: Data curation, Investigation.

Competing interests

The contact author has declared that none of the authors has any competing interests.

https://doi.org/10.5194/essd-2026-398
Preprint. Discussion started: 11 June 2026

Open Access Earth System Science Data Discussions

Disclaimer

Publisher's note: Copernicus Publications remains neutral with regard to jurisdictional claims in published maps and institutional affiliations.

Acknowledgements

The authors are grateful to the China Argo Real - time Data Center for providing us with the near - real - time observations and to the Copernicus Marine Service for the satellite remote sensing data. We also acknowledge all the colleagues and project members who have contributed to the design of EFGO, the sea experiments, and data processing in the past. Many scientists, engineers, and students have actively participated in surveys and mappings.

Financial support

This study was financially supported in part by the General Program of the National Natural Science Foundation of China under Grant 42576203, and in part by the Program on the Survey, Monitoring and Assessment of Global Fishery Resources (Comprehensive scientific survey of fisheries resources at the high seas) sponsored by the Ministry of Agriculture and Rural Affairs under Grant D-8025-25-5001.

References

1. Asdar, S., Ciani, D., and Nardelli, B. B.: 3D reconstruction of horizontal and vertical quasi-geostrophic currents in the North Atlantic Ocean, Earth Syst. Sci. Data, 16, 1029-1046, https://doi.org/10.5194/essd-16-1029-2024, 2024.
2. Chaigneau, A., Le Texier, M., Eldin, G., Grados, C., and Pizarro, O.: Vertical structure of mesoscale eddies in the eastern south pacific ocean: a composite analysis from altimetry and argo profiling floats, J. Geophys. Res.-Oceans, 116, C11025, https://doi.org/10.1029/2011JC007134, 2011.
3. Chaubell, J., Chan, S., Dunbar, R., Entekhabi, D., Peng, J., Piepmeier, J., and Yueh, S.: Backus-gilbert optimal interpoaltion applied to enhance SMAP data: Implementation and assessment, 2017 IEEE International Geoscience and Remote Sensing Symposium (IGARSS), Fort Worth, TX, USA, 23-28 July 2017, 2531-2534, https://doi.org/10.1109/IGARSS.2017.8127510, 2017.
4. Dong, D., Brandt, P., Chang, P., Schütte, F., Yang, X. F., Yan, J. H., Zeng, J. S.: Mesoscale Eddies in the Northwestern Pacific Ocean: Three-Dimensional Eddy Structures and Heat/Salt Transports, Journal of Geophysical Research Oceans, 122, 9795-9813, https://doi.org/10.1002/2017JC013303, 2017.
5. Falkowski, P. G.,Ziemann, D., Kolber, Z. , and Bienfang P. K.: Role of eddy pumping in enhancing primary production in the ocean, Nature, 352, 55–58, https://doi.org/10.1038/352055a0, 1991.
6. Gandin, L.S.: Objective analysis of meteorological fields, Quarterly Journal of the Royal Meteorological Society, 92, 447, https://doi.org/10.1002/qj.49709239320, 1996.
7. He, Q. Y., Zhan, H. G., Cai, S. Q., He, Y. H., Huang, G. L., and Zhan, W. K.: A new assessment of mesoscale eddies in the south china sea: surface features, threedimensional structures, and thermohaline transports, J. Geophys. Res.-Oceans., 123, 4906-4929, https://doi.org/10.1029/2018JC014054, 2018.
8. Kalnay, E.: Atmospheric modeling, data assimilation, and predictability, Cambridge University Press, London, UK, 129 pp., ISBN: 9780511802270, 2012.

https://doi.org/10.5194/essd-2026-398
Preprint. Discussion started: 11 June 2026

9. Klein, P., and Lapeyre, G.: The oceanic vertical pump induced by mesoscale and submesoscale turbulence, Annu. Rev. Mar. Sci., 1, 351–375, https://doi.org/10.1146/annurev.marine.010908.163704, 2009.
10. Liu, Z. H., Li, Z. Q., Lu, S. L., Wu, X. F., Sun, C. H., and Xu, J. P.: Scattered Dataset of Global Ocean Temperature and Salinity Profiles from the International Argo Program, Journal of Global Change Data & Discovery, 5: 22–31, https://doi.org/10.3974/geodp.2021.04.03, 2021.
11. Ma, Y., Liu, W., Huang, B. X., Tian, F. L., and Chen, G.: EFGAN: An automatic GAN-based methodology for mining eddy-front coupling with fused remote sensing data, Information Fusion, 101, 101982, https://doi.org/10.1016/j.inffus.2023.101982, 2024.
12. Ma, Y., Tian, F. L., Long, S., Huang, B. X., Liu, W., and Chen, G.: Global Oceanic Eddy-Front Associations From Synergetic Remote Sensing Data by Deep Learning, IEEE Geoscience and Remote Sensing Letters, 20, 1-5, https://doi.org/10.1109/LGRS.2023.3310053, 2023.
13. Ma, Z. T., Huang, L. Y., Yang, J. S., Ren, L., Li, X. H., He, S. Y., Liu, B. Q., and Liu, A. K.: Transformer-Based Hierarchical Multiscale Feature Fusion Internal Wave Detection and Dataset, Ocean-Land-Atmosphere Research, 3, 0061, https://spj.science.org/doi/10.34133/olar.0061, 2024.
14. McWilliams, J. C.: Submesoscale currents in the ocean, P. R. Soc. A-Math. Phy., 472, 20160117, https://doi.org/10.1098/rspa.2016.0117, 2016.
15. Okkonen, S. R., Weingartener, T. J., Danielson, S. L., Musgrave, D. L., and Schmidt, G. M.: Satellite and hydrographic observations of eddy-induced shelf-slope exchange in the northwestern Gulf of Alaska, J. Geophys. Res., 108, 3033, https://doi.org/10.1029/2002JC001342, 2003.
16. Sandalyuk, N.V., Bosse, A., Belonenko, T.V.: The 3D structure of mesoscale eddies in the Lofoten basin of the Norwegian sea: a composite analysis from altimetry and in situ data, J. Geophys. Res.-Oceans, 125, e2020JC016331, https://doi.org/10.1029/2020JC016331, 2020.
17. Scott, R. M., Pickart, R. S., Lin, P., Münchow, A., Li, M., Stockwell, D. A., and Brearley, J. A.: Three-dimensional structure of a cold-core arctic eddy interacting with the Chukchi slope current, J. Geophys. Res.-Oceans, 124, 8375–8391, https://doi.org/10.1029/2019JC015523, 2019.
18. Wang, P. H., Mao, K. F., Chen, X., Li, M., Zhu, Y. H., Li, H. C., Wang, J. H., Liu, K. F., and Wang, Y. J.: Three-dimensional structure reconstruction of ocean mesoscale eddies based on physical process modeling and data-driven machine learning, Ocean Modelling, 196, 102558, https://doi.org/10.1016/j.ocemod.2025.102558, 2025.
19. Xing, Q. W., Yu, H. Q., Yu, W., Chen, X. J., and Wang, H.: A global daily mesoscale front dataset from satellite observations: In situ validation and cross-dataset comparison, Earth System Science Data, 17, 2831-2848, https://doi.org/10.5194/essd-17-2831-2025, 2025.
20. Yang, G., Wang, F., Li, Y. L., and Lin, P. F.: Mesoscale eddies in the northwestern subtropical pacific ocean: statistical characteristics and three-dimensional structures, J. Geophys. Res.: Oceans, 118, 1906–1925, https://doi.org/10.1002/jgrc.20164, 2013.
21. Zhang, C. L., Sun, A. R., Mao, K. F., Liu, Z. H., Wang, P. H., Fu, L. F., Zhu, Y. H., and Fan, J. H.: EFGO:High-Resolution Eddy Model Fusion Gradient Optimal Interpolation Data (Version v1) [Data set]. Zenodo. https://doi.org/10.5281/zenodo.20396796, 2026.
22. Zhang, C. L., Xu, J. P., Bao, X. W., and Wang, Z. F.: An effective method for improving the accuracy of Argo objective analysis, Acta Oceanologica Sinica, 32, 66-77, https://doi.org/10.1007/s13131-013-0333-1, 2013.
23. Zhang, C.L., Wang, Z.F., and Liu,Y.: An Argo-based experiment providing near-real-time subsurface oceanic environmental information for fishery data, Fish. Oceanogr., 30, 85–98, https://doi.org/10.1111/fog.12504, 2021.
24. Zhang, C. L., Wang, D. Y., and Wang, Z. F.: Fishery analysis using gradient-dependent optimal interpolation, Acta Oceanologica Sinica, 41, 116-126, https://doi.org/10.1007/s13131-021-1895-y, 2022.

https://doi.org/10.5194/essd-2026-398
Preprint. Discussion started: 11 June 2026

25. Zhang, L., Ma, X. D., Wan, X., Xu, W. S., Sun, X. Q., and Li, M. L.: Three-dimensional thermohaline reconstruction of mesoscale eddies under remote sensing observation: From the perspective of deep learning of layer depth sequences with fusion of physical mechanisms, Journal of Sea Research, 205, 102593, https://doi.org/10.1016/j.seares.2025.102593, 2025.
26. Zhang, X. M., Huang, B. X., and Chen, G.: Dynamic evolution mechanism driven lifetime prediction for global mesoscale eddy, Big Earth Data, 9, 1058-1085, https://doi.org/10.1080/20964471.2025.2560750, 2025.
27. Zhang, Z. G., Zhang, Y., Wang, W., and Huang, R.X.: Universal structure of mesoscale eddies in the ocean, Geophys. Res. Lett., 40, 3677–3681, https://doi.org/10.1002/grl.50736, 2013.
28. Zhang, Z. W., Tian, J. W., Qiu, B., Zhao, W., Chang, P., Wu, D. X., and Wan, X. Q.: Observed 3d structure, generation, and dissipation of oceanic mesoscale eddies in the south China sea, Sci. Rep., 6, 24349, https://doi.org/10.1038/srep24349, 2016.
29. Zhu, Q. S., Li, H. P., Sun, H. C., Xia, T. Y., Wang, X. M., and Han, Z. J.: 3DV-Unet: Eddy-Resolving Reconstruction of Three-Dimensional Upper-Ocean Physical Fields from Satellite Observations, Remote Sens, 17, 3394, https://doi.org/10.3390/rs17193394, 2025.